Applying Machine Learning based on Multiscale Classifiers to Detect Remote Phenology Patterns in Cerrado Savanna Trees

Jurandy Almeida[a,*], Jefersson A. dos Santos[a], Bruna Alberton[b], Ricardo da S. Torres[a], Leonor Patricia C. Morellato[b]

[a] *RECOD Lab, Institute of Computing, University of Campinas – UNICAMP*
13083-852, Campinas, SP – Brazil
[b] *Phenology Lab, Dept. of Botany, Sao Paulo State University – UNESP*
13506-900, Rio Claro, SP – Brazil

Abstract

Plant phenology is one of the most reliable indicators of species responses to global climate change, motivating the development of new technologies for phenological monitoring. Digital cameras or near remote systems have been efficiently applied as multi-channel imaging sensors, where leaf color information is extracted from the RGB (Red, Green, and Blue) color channels, and the changes in green levels are used to infer leafing patterns of plant species. In this scenario, texture information is a great ally for image analysis that has been little used in phenology studies. We monitored leaf-changing patterns of a cerrado-savanna vegetation by taken daily digital images. We extract RGB channels from digital images and correlated with phenological changes. Additionally, we benefit from the inclusion of textural metrics for quantifying spatial heterogeneity. Our first goals are: (1) to test if the color change information is able to characterize the phenological pattern of a group of species; (2) to test if the temporal variation in image texture is useful to distinguish plant species; and (3) to test if individuals from the same species may be automatically identified using digital images. In this paper, we present a machine learning approach based on multiscale classifiers to detect phenological patterns in the digital images. Our results indicate that: (1) extreme hours (morning and afternoon) are the best for identifying plant species; (2) different plant species present a different behavior with respect to the color change information; and (3) texture variation along temporal images is a promising information for capturing phenological patterns. Based on those results, we suggest that individuals from the same species and functional group might be identified using digital images, and introduce a new tool to help phenology experts in the identification of new individuals from the same species in the image and their location on the ground.

Keywords: remote phenology, digital cameras, machine learning, image analysis, tropical forests

1. Introduction

Phenology, the study of natural recurring phenomena and its relation to climate (Schwartz, 2003), is a traditional science dedicated to the observation of the cycles of plants and animals and relate mainly to local meteorological data, as well as to biotic interactions and phylogeny (Staggemeier et al., 2010).

The leaf exchange patterns from leaf flush to senescence are key events to understand a range of ecosystem processes, considering its prominence on growth, water status, gas exchange, and nutrient cycling (Negi, 2006; Reich, 1995). The carbon balance and the productivity of terrestrial ecosystems are essentially defined by the dynamics of plant growing seasons (Keeling et al., 1996; Loustau et al., 2005; Rotzer et al., 2004), controlling spatial and temporal patterns of carbon and water exchange between forest and atmosphere (Schwartz et al., 2002; White et al., 1999).

Plant phenology has gained importance as the simplest and most reliable indicator of species responses in the context of global change research, stimulating the development of new technologies for phenological observation (Parmesan and Yohe, 2003; Richardson et al., 2009; Rosenzweig et al., 2008; Walther, 2004; Walther et al., 2002). Digital cameras have been suc-

---

*Corresponding author. Tel.: +55 19 3521-5887; Fax: +55 19 3521-5847

Email addresses: `jurandy.almeida@ic.unicamp.br` (Jurandy Almeida), `jsantos@ic.unicamp.br` (Jefersson A. dos Santos), `bru.alberton@gmail.com` (Bruna Alberton), `rtorres@ic.unicamp.br` (Ricardo da S. Torres), `pmorella@rc.unesp.br` (Leonor Patricia C. Morellato)

cessfully used as multi-channel imaging sensors, and the measurements of color change information (RGB channels) from digital images allow to detect phenological changes in plants (Ahrends et al., 2009; Ide and Oguma, 2010; Kurc and Benton, 2010; Nagai et al., 2011; Richardson et al., 2009, 2007).

After quantifying the color channels, it is possible to estimate changes on phenological events, such as leaf flushing when analyzing the green channel, or leaf color change and senescence using values from the red channel (Ahrends et al., 2009; Richardson et al., 2009). However, image information from digital camera is sparse for high diverse tropical forest, where one image may encompass dozens to more than a hundred species, compared to the low number of species on temperate vegetations.

Another important feature that can be extracted from digital images is the spatial arrangement of the pixel intensities, known as texture (Torres and Falcão, 2006). The appearance of texture can help an observer to determine whether different regions from a digital image of a given vegetation have a same structure. Due to difficulties in measurement and interpretation, texture has been little used in phenology studies (Culbert et al., 2009).

We monitored a tropical cerrado savanna vegetation to accesses the reliability of digital images to detect leaf changes and validate the digital data with on the ground direct phenological observation (Alberton et al., 2012). In this paper, we investigate the use of machine learning based on multiscale classifiers to detect phenological patterns in a cerrado savanna by using color and texture information of digital images. The key contribution of this study is the analysis of intra-species variations.

The primary goal of our research is to determine how good is the color change information to characterize the phenological pattern of a group of species. Moreover, we are interested in analyzing how promising is the temporal variation in image texture to distinguish different individuals that have similar spectral characteristics but different spatial patterns. Finally, we use machine learning based on multiscale classifiers to find similar textures in the digital image and we checked if they correspond to similar species or functional groups.

Based on those studies, we expect to open new venues on the automatic identification of plants from the same species or functional group using machine learning. Most of existing methods for species identification have focused on morphological features of a single organ (mainly leaf, rarely flower), often considering ideal conditions, such as noise-free images with a uniform background, taken at specific periods (Cope et al., 2012; Kumar et al., 2012).

Unlike previous works in the literature, we address the problem of identifying plant species by using phenology instead of morphometrics. Our strategy integrates a high degree of diversity in terms of locations, periods, and illumination conditions, which is a prerequisite to build modern plant identification systems.

A preliminary version of this work was presented at eScience 2012 (Almeida et al., 2012). Here, we include the analysis of texture information to characterize phenological patterns. The new reported results show the potential of texture change information for species identification.

The remainder of this paper is organized as follows. Section 2 presents our learning strategy and shows how to apply it to identify plant species. Section 3 describes materials and methods of our experimental protocol. Section 4 reports our experimental results and discuss how they can be applied in phenology studies. Finally, we offer our conclusions and directions for future work in Section 5.

2. Machine Learning

In machine learning, classification is the task of assigning objects to one of several predefined *classes*. The input data for a classification task is a collection of records. Each record, also known as a *sample*, is characterized by a tuple $(\mathcal{F}, Y)$, where $\mathcal{F}$ is the attribute set and Y is a special attribute, called *label*, which indicates the class that belongs each sample (Tan et al., 2005).

The attribute set $\mathcal{F}$, also known as a *feature vector*, is a sequence of continuous or discrete values obtained from measures over a given object and it is used for computationally describe each sample concerning a specific property. The label, on the other hand, must be a discrete attribute (Tan et al., 2005).

A *detector* or *classifier* is a systematic approach to building classification models from an input data set. Each technique employs a *learning strategy* to identify a model that best fits the relationship between the feature vector and label of the input data (Tan et al., 2005).

For that, a *training set* consisting of records whose labels are known must be provided. The training set is used to build a classification model, which is subsequently applied to predict the labels of records it has never seen before (Tan et al., 2005). For more details concerning machine learning concepts, refer to (Alpaydin, 2010; Rostamizadeh and Talwalker, 2012).

In this paper, we use machine learning to detect phenological patterns. For this purpose, we adopted the *multiscale classifier* (MSC) approach (dos Santos et al.,

2012b) to learn phenological patterns and build phenological pattern detectors. It was chosen due to its ability of combining different features by weighting the ones more suitable for each plant species. Moreover, it also allows the combination of features from different segmentation scales, which increases the power of the final detector (dos Santos et al., 2012a).

2.1. Multiscale classifier

The *multiscale classifier* (MSC) (dos Santos et al., 2012b) is a learning strategy based on boosting of weak learners. It is based on the Adaboost algorithm proposed by Schapire (1999), which builds a linear combination of weak classifiers to compose a final strong one. A weak learner is a classifier slightly better than the random. Boosting-based classification strategies have been extensively used in applications that need to combine a large sets of different features or classifiers (Grabner and Bischof, 2006; Lechervy et al., 2013; Viola and Jones, 2001).

Let H be a hierarchy of segmented regions, P_λ is a partition, which is the segmentation result at a given scale λ. A partition P is obtained by cutting the hierarchy H. In this sense, $R \in P$ refers to any region R that belongs to the partition P. The MSC aims at assigning a label (+1, for relevant class; and −1, otherwise) to each pixel p of P_0 taking advantage of various features computed on regions of various levels from a segmentation hierarchy H. The final classifier is a linear combination $MSC(p)$ of T weak classifiers $h_t(p)$:

$$MSC(p) = \text{sign}\Big(\sum_{t=1}^{T} \alpha_t h_t(p) \Big), \qquad (1)$$

where α_t is the weight assigned to the weak classifier $h_t(p)$ at the iteration t.

The training consists in testing *weak learners* in a sequence of rounds $t = 1, \ldots T$. Each weak learner builds a weak classifier that reduces the expected classification error of the final classifier. For each round t, MSC selects the weak classifier that most decreases the error.

The algorithm keeps a set of weights over the training set. The weights can be understood as a measure of difficulty of each sample. The pixels starts with the same weight. But along the rounds, the weights of the misclassified pixels are increased. Thus, the weak learners are forced to focus on the most difficult samples. We note $W_t(p)$ the weight of pixel p in round t, and $D_{t,\lambda}(R)$ the misclassification rate of region R in round t at scale λ which is the mean of the weights of its pixels:

$$D_{t,\lambda}(R) = \Big(\frac{1}{|R|} \sum_{p \in R} W_t(p) \Big). \qquad (2)$$

Algorithm 1 presents the training process of the MSC. Let $Y_\lambda(R)$, the set of labels of regions R at scale λ, be the training set. In a series of rounds $t = 1, \ldots T$, for all scales λ, the weight of each region $D_{t,\lambda}(R)$ is computed (line 3). The selection of regions is based on this piece of information and to create a subset of labeled regions $\hat{Y}_{t,\lambda}$ (line 6). This subset is used to train weak learners: each features $\mathcal{F}$ at scale λ (line 9). Each weak learner produces a weak classifier $h_{t,(\mathcal{F},\lambda)}$ (line 10). The algorithm then selects the weak classifier h_t that most reduces the error Err_{h_t} (line 12). The level of error of h_t is used to compute the coefficient α_t, which indicates the degree of importance of h_t in the final classifier (line 13). The selected weak classifier h_t and the coefficient α_t are used to update the weights of the pixels $W_{(t+1)}(p)$ which can be used in the next round (line 14).

Algorithm 1 Multiscale Classifier

Input:

    Training labels $Y_\lambda(R)$ = labels of regions R at scale λ

Initialize:

    For all pixels p, $W_1(p) \leftarrow \frac{1}{|Y_0|}$, where $|Y_0|$ is the number of pixels in the image level

1   For $t \leftarrow 1$ to T do
2   For all scales λ do
3   For all $R \in P_\lambda$ do
4   Compute $D_{t,\lambda}(R)$
5   End for
6   Build $\hat{Y}_{t,\lambda}$ (a training subset based on $D_{t,\lambda}(R)$)
7   End for
8   For each pair feature/scale $(\mathcal{F}, \lambda)$ do
9   Train *weak learners* using features $(\mathcal{F}, \lambda)$ and training set $\hat{Y}_{t,\lambda}$.
10   Evaluate resulting classifier $h_{t,(\mathcal{F},\lambda)}$: compute $Err(h_{t,(\mathcal{F},\lambda)}, W))$ (Equation 3)
11   End for
12   Select *weak classifier* $h_t = \text{argmin}_{h_{t,(\mathcal{F},\lambda)}} Err(h_{t,(\mathcal{F},\lambda)}, W_{t,\lambda})$
13   Compute $\alpha_t \leftarrow \frac{1}{2} ln\Big(\frac{1+r_t}{1-r_t}\Big)$ with $r_t \leftarrow \sum_p c Y_0(p) h_t(p)$
14   Update $W_{t+1}(p) \leftarrow \dfrac{W_t(p) \exp\left(-\alpha_t Y_0(p) h_t(p)\right)}{\sum\limits_p W_t(p) \exp\left(-\alpha_t Y_0(p) h_t(p)\right)}$
15   End for

Output: Multi-Scale Classifier $MSC(p)$

3

The training set labels Y_0 corresponds to the samples at the pixel level. The training sets labels Y_λ with $\lambda > 0$ are defined according to the percentage of pixels that belongs to each of the two classes (for example, at least 80% of one region). The learning is performed over a training set Y_λ corresponding to the same scale λ. The weak learners use the subset $\hat{Y}_{t,\lambda}$ for training and produce a weak classifier $h_{t,(\mathcal{F},\lambda)}$.

The classification error of the classifier h is:

$$Err(h, W) = \sum_{p | h(p) Y_0(p) < 0} W(p). \qquad (3)$$

2.2. SVM-based weak learner

In this work, we used a linear SVM (support vector machine) as weak learner, which is an SVM trainer based on a specific feature type $\mathcal{F}$ and a specific scale λ. Given the training subset labels $\hat{Y}_\lambda$, the method finds the best linear hyperplane of separation, trying to maximize the data separation between the regions according to their classes. The sample regions in the margin are called support vectors and are found during the training.

Once the support vectors and the decision coefficients ($\alpha_i, i = 1, \ldots, N$) are found, the SVM weak classifier can be defined as:

$$SVM_{(\mathcal{F},\lambda)}(R) = \text{sign}\Big(\sum_i^N y_i \alpha_i (f_R \cdot f_i) + b \Big), \qquad (4)$$

where b is a parameter found during the training. The support vectors are the f_i such that $\alpha_i > 0$, y_i is the support vector class and f_R is the feature vector of the region.

Only the most difficult regions are supposed to be used for training. Thus, the training subset $\hat{Y}_{t,\lambda}$ is composed by n labels from Y_λ with values of $D_{t,\lambda}(R)$ larger or equal to $\frac{1}{|Y_0|}$.

3. Materials and Methods

3.1. Study Area and Camera Setup

The near-remote phenological system was set up in a 18m tower in a Cerrado *sensu stricto*, a savanna-like vegetation located at Itirapina (22° 10' 49.18" S / 47° 52' 16.54" O), São Paulo State, Brazil. The cerrado stricto sensu (Coutinho, 1978) is a savanna-like vegetation presenting a discontinuous canopy and woody component reaching six to seven meters high and a continuous herbaceous layer (Alberton et al., 2012). In some parts, the vegetation is denser, with some trees reaching up to 12 m high. The cerrado savanna study site is about 260 ha, 610 m altitude and the regional climate is Cwa type (i.e., humid subtropical climate) according to Köppen classification.

The average climate (1972 to 2002) shows a mean annual total rainfall of 1524 mm and mean temperature of 20.7 °C, with one warm, humid season from October to March (average of 22 °C and 78% of annual precipitation) and one cool, dry season from April to September (average of 18 °C and 16% of annual precipitation). During the year of study (2011) the climate seasonality was similar to the average pattern, with a mean temperature of 21.2 °C, but a higher annual total rainfall of 1891 mm due to a very humid January with precipitation over 500 mm. Climatic data were obtained from the Climatological Station of the Center for Water Resources and Applied Ecology (CRHEA) of the University of Sao Paulo, located 4 km from the study site.

A digital hemispherical lens camera (Mobotix Q24) was setup at the top of the phenology tower, attached in an iron arm facing northeast (Figure 1). The camera activity is controlled by a timer and the energy source is a 12 V battery charged by a solar panel.

Figure 1: The cerrado-savanna phenology tower (18m tall) at Itirapina, São Paulo, Southeastern Brazil, where the digital hemispherical lens camera was set up (red arrow) attached in an iron arm facing northeast.

The first data collection from the digital camera started on 18th August 2011. We set up the camera to automatically take a daily sequence of five JPEG images (at 1280×960 pixels of resolution) per hour, from 6:00 to 18:00 h (UTC-3). The present study was based on the analysis of over 2,700 images (Figure 2), recorded at the end of the dry season, between August 29th and October 3rd 2011, day of year 241 to 278 (DOY), during the main leaf flushing season (Alberton et al., 2012; Reys, 2008). Sunrise, sunset, and solar elevation angle were 6:03 h, 17:38 h, 58° (DOY 241); and 5:26 h, 17:48 h, 72° (DOY 278), respectively.
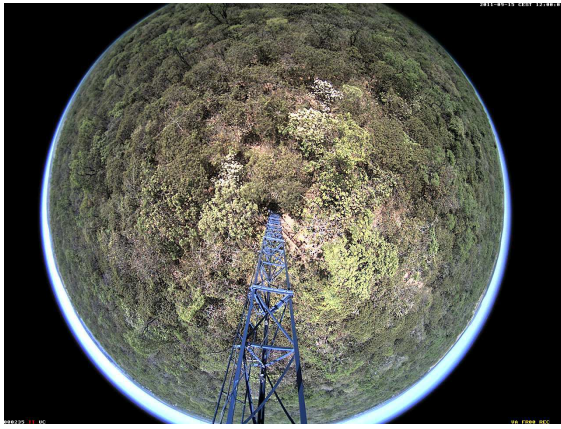

Figure 2: Sample image of the cerrado savanna recorded by the digital camera on October 15th, 2011.

3.2. Image Analysis

3.2.1. Regions of Interest

The image analysis was conducted by defining different regions of interest (ROI), as described by Ahrends et al. (2009); Alberton et al. (2012); Richardson et al. (2009, 2007). For each ROI, a binary image with the same dimensions of the original image was created as a mask. White pixels of a mask indicate the ROI, while the remaining area was filled by black pixels. We defined six ROIs (Figure 3) based on the random selection of six plant species identified manually by phenology experts in the hemispheric image: (1) *Aspidosperma tomentosum* (Figure 3(a)), (2) *Caryocar brasiliensis* (Figure 3(b)), (3) *Myrcia guianesis* (Figure 3(c)), (4) *Miconia rubiginosa* (Figure 3(d)), (5) *Pouteria ramiflora* (Figure 3(e)), and (6) *Pouteria torta* (Figure 3(f)).

According to the leaf exchange data from the on-the-ground field observations on leaf fall and leaf flush at our study site, those species were classified on three functional groups (Alberton et al., 2012; Morellato

et al., 1989; Reys, 2008): (i) deciduous, *Aspidosperma tomentosum* and *Caryocar brasiliensis*; (ii) evergreen, *Myrcia guianensis* and *Miconia rubiginosa*; and (iii) semideciduous, *Pouteria ramiflora* and *Pouteria torta*.

3.2.2. Color Features

We analyzed each ROI in terms of the contribution of the primary colors (Red, Green, and Blue), as proposed by Richardson et al. (2007). Initially, a custom script was used to analyze each color channel and to compute the average value of the pixel intensity. After that, we calculated the relative (or normalized) brightness of each color channel, as:

$$Total_{avg.} = Red_{avg.} + Green_{avg.} + Blue_{avg} \quad (5)$$
$$\% \, of \, Red = \frac{Red_{avg.}}{Total_{avg.}}$$
$$\% \, of \, Green = \frac{Green_{avg.}}{Total_{avg.}}$$
$$\% \, of \, Blue = \frac{Blue_{avg.}}{Total_{avg.}}$$

where $Red_{avg.}$, $Green_{avg.}$, and $Blue_{avg.}$ are the average pixel intensity of the red, green, and blue bands, respectively. The normalization of those values reduces the influence of the incident light, decreasing the color variability due to changes on illumination conditions (Cheng et al., 2001).

Figure 4 shows the behavior of those values for each ROI along the whole period, considering only the digital images taken at the midday. Each line corresponds to a time series for the variation of the normalized brightness of each color channel. Notice the differences between the behavior of each species individually, reflecting the leaf color changes over the leaf life cycle or aging process.

3.2.3. Texture Features

One of the most traditional techniques for extracting and representing texture information is the Co-occurrence matrix (Haralick et al., 1973). It describes spatial relationships among pixel intensities in an image. Each position (i, j) in this matrix indicates the probability at which pixels of intensity values i and j occur at a user specified distance and direction. There are four commonly used directions: 0° (horizontal), 45° (right diagonal), 90° (vertical), and 135° (left diagonal). The distance parameter is typically set to 1, thus comparing adjacent pixels. From this matrix, we can compute properties such as contrast, entropy, and homogeneity.

(a) *Aspidosperma tomentosum*

(b) *Caryocar brasiliensis*

(c) *Myrcia guianesis*

(d) *Miconia rubiginosa*

(e) *Pouteria ramiflora*
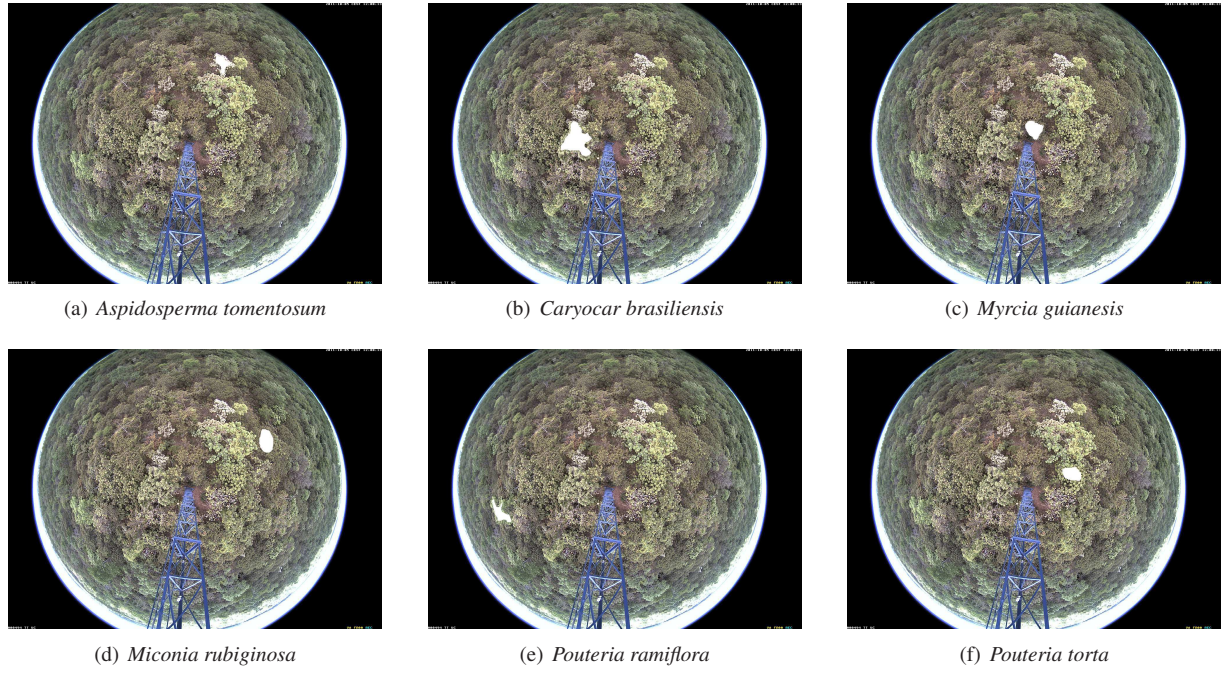
(f) *Pouteria torta*

Figure 3: Regions of interest (ROIs) defined for the analysis of cerrado-savanna digital images: (a) *Aspidosperma tomentosum*, (b) *Caryocar brasiliensis*, (c) *Myrcia guianesis*, (d) *Miconia rubiginosa*, (e) *Pouteria ramiflora*, and (f) *Pouteria torta*.

(a) *Aspidosperma tomentosum*

(b) *Caryocar brasiliensis*

(c) *Myrcia guianesis*

(d) *Miconia rubiginosa*

(e) *Pouteria ramiflora*

(f) *Pouteria torta*

Red ——— Green ——— Blue ———
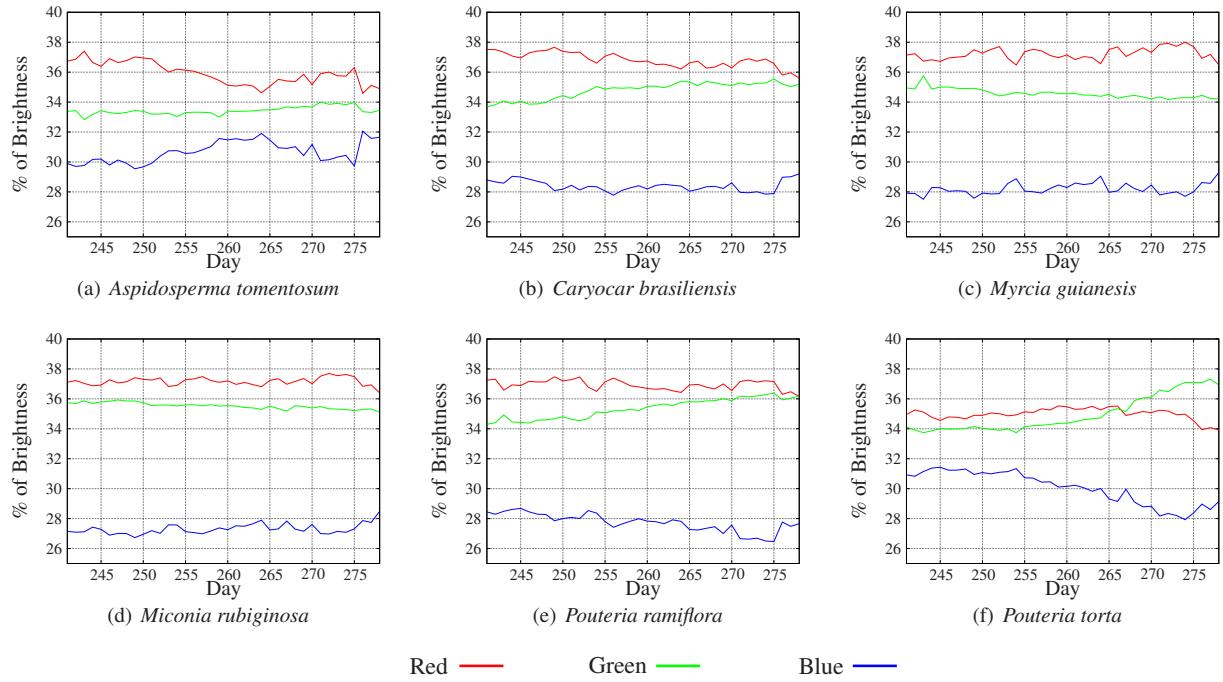
Figure 4: The variance of the normalized brightness of each color channel from the digital images taken at the midday, each Julian day (August 28th to October 3rd, 2011), in the cerrado savanna using different regions of interest (ROIs), as described in Figure 3.

6

A simplification of the aforementioned method consists in replacing the usual co-occurrence matrices by their associated sum and difference histograms (Unser, 1986). The non-normalized sum s and difference d associated with a relative displacement (δ_1, δ_2) on the position (k, l) of an image I are defined as:

$$s_{k,l} = I_{k,l} + I_{k+\delta_1, l+\delta_2}, \tag{6}$$
$$d_{k,l} = I_{k,l} - I_{k+\delta_1, l+\delta_2}.$$

Let D be a subset of indexes specifying a region to be analyzed and $G = \{1, 2, \ldots, N_g\}$ be the set of the N_g pixel levels. The sum (h_s) and difference (h_d) histograms for the intensity values i and j over the domain D are defined by:

$$h_s(i; \delta_1, \delta_2) = h_s(i) = Card\{(k,l) \in D, s_{k,l} = i\}, \tag{7}$$
$$h_d(j; \delta_1, \delta_2) = h_d(j) = Card\{(k,l) \in D, d_{k,l} = j\}.$$

The normalized sum (P_s) and differences (P_d) histograms are given by

$$P_s(i) = h_s(i)/N \qquad i = 2, \ldots, 2N_g, \tag{8}$$
$$P_d(j) = h_d(j)/N \quad j = -N_g + 1, \ldots, N_g - 1,$$

where N is the total number of counts,

$$N = Card\{D\} = \sum_i h_s(i) = \sum_j h_d(j). \tag{9}$$

Statistical information can be extracted from those histograms by computing quantities such as mean, variance, and entropy. Unser (1986) has presented a variety of statistical measures that can be employed to extract useful information from both sum and difference histograms, as shown in Table 1. Such measures were computed from the sum and difference histograms obtained from the green color band by considering the domain D defined by each ROI.

Table 1: Textural metrics extracted from each ROI.

Feature	Formula
Mean	$\mu = \frac{1}{2} \sum_i i \cdot P_s(i)$
Contrast	$C_n = \sum_j j^2 \cdot P_d(j)$
Homogeneity	$H_g = \sum_j \frac{1}{1+j^2} \cdot P_d(j)$
Variance	$\sigma^2 = \frac{1}{2}\left(\sum_i (i - 2\mu)^2 \cdot P_s(i) + \sum_j j^2 \cdot P_d(j)\right)$
Correlation	$C_r = \frac{1}{2}\left(\sum_i (i - 2\mu)^2 \cdot P_s(i) - \sum_j j^2 \cdot P_d(j)\right)$
Entropy	$H_n = -\sum_i h_s(i) \cdot \log P_s(i) - \sum_j P_d(j) \cdot \log P_d(j)$
Maximum	$M_p = \max_i P_s(i)$

Figure 5 shows the behavior of those measures for each ROI along the whole period, considering only the digital images taken at the midday. Each line corresponds to a time series for the variation of the normalized value of each textural metric. The behavior of those curves is equivalent for the different orientations. For that reason, we report the average results of the all the directions (0°, 45°, 90°, and 135°).

3.3. Classification

Figure 6 illustrates the steps of our MSC approach. The first step is to build a hierarchy of regions H. We have used Guigues algorithm (Guigues et al., 2006) to perform the segmentation. In the remainder of this paper, when we refer to regions of interest related to tree crowns of plant species identified manually in the digital image, we use the acronym ROI; and when we refer to segmented regions obtained from the segmentation algorithm, we use the acronym SR.

The image used to obtain the hierarchy of segmented regions (SR) was taken at noon on October 15th, 2011 (Figure 2). We have selected 5 segmentation scales from the hierarchy to perform feature extraction. The finest scale is composed of $27,380$ SRs and the coarsest scale contains $8,849$ SRs. Figure 7 illustrates the segmented scales in a subimage sample from Figure 2.
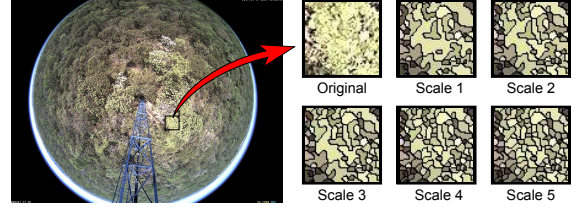

Figure 7: The segmentation results for the selected scales in a subimage sample.

The second step is the feature extraction, which is carried out on the SRs at different segmentation scales. For each plant species, we have tested 39 different color features by considering the available periods during the day (13 hours: from 6:00 to 18:00 h) and the color channels (3 bands: R, G, and B). Also, we have tested 91 different texture features by considering the available periods during the day (13 hours: from 6:00 to 18:00 h) and the texture metrics (7 statistical measures: mean, variance, contrast, correlation, entropy, homogeneity, and maximum probability). For each feature, we take the average value obtained for the five images of each hour of the day. Time series are obtained by computing those values along the whole period (August 28th to October 3rd, 2011), forming the feature vector.

Finally, we use the MSC (Algorithm 1) to build a linear combination of weak classifiers, each of them related to a specific scale and feature. This step was performed for each plant species by using their ROIs (Figure 3). To build a classifier for a given species, we used the SRs from its corresponding ROI as positive samples and from ROIs of the other species as negative samples. At the end, the final classifier was applied to classify the remaining SRs of the image.

(a) *Aspidosperma tomentosum* (b) *Caryocar brasiliensis* (c) *Myrcia guianesis*

(d) *Miconia rubiginosa* (e) *Pouteria ramiflora* (f) *Pouteria torta*

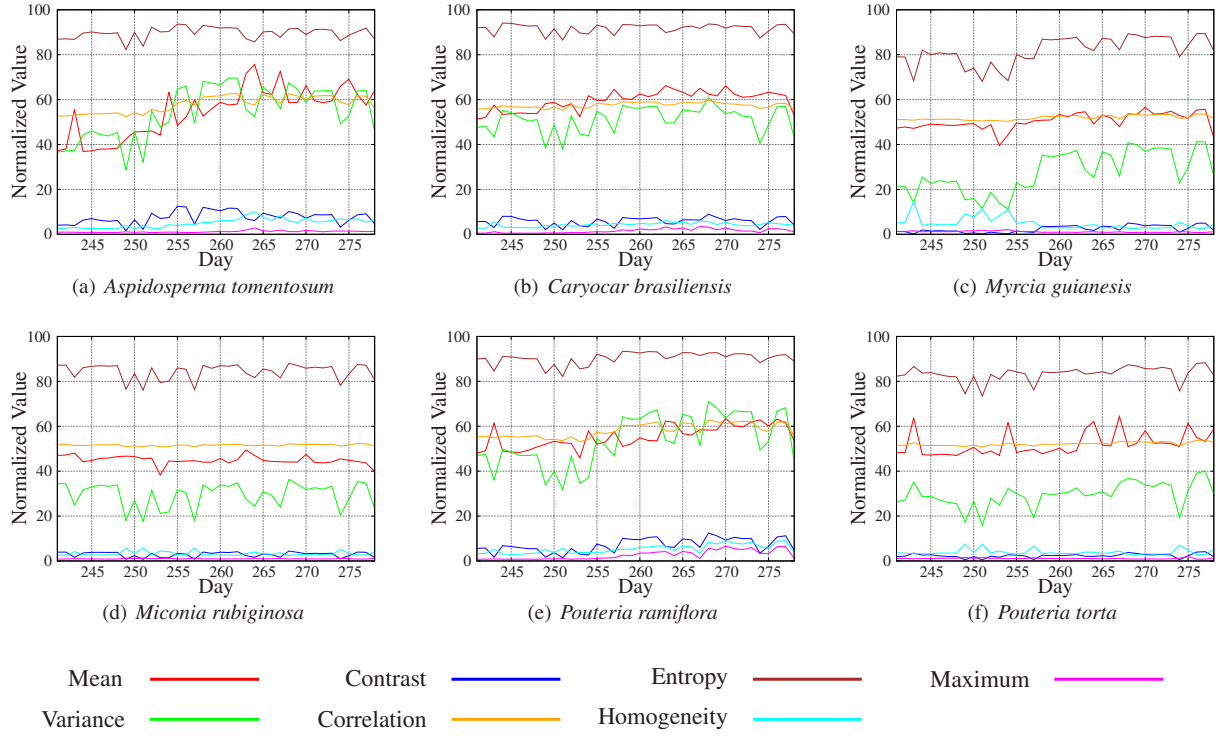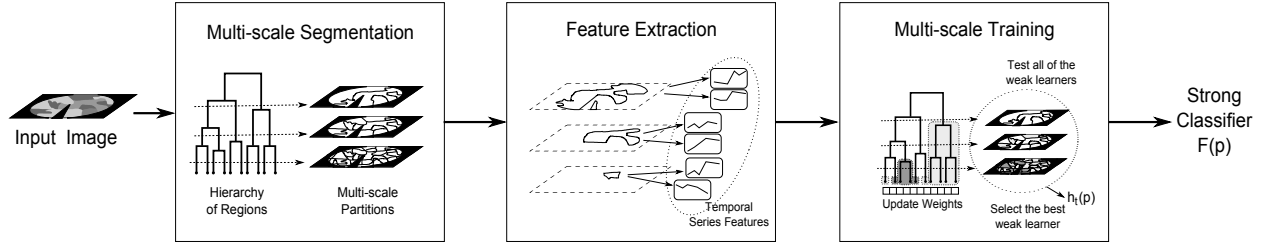| Mean | Contrast | Entropy | Maximum |
| Variance | Correlation | Homogeneity | |

Figure 5: The variance of the normalized value of each textural metric from the digital images taken at the midday, each Julian day (August 28th to October 3rd, 2011), in the cerrado savanna using different regions of interest (ROIs), as described in Figure 3.

Figure 6: Steps of the multi-scale learning process. Adapted from dos Santos et al. (2012b).

3.4. Effectiveness Measures

We carried out experiments to classify the plant species in the image. For that, we selected two species from different functional groups: *Aspidosperma tomentosum* (deciduous) and *Miconia rubiginosa* (evergreen). Next, we built a classifier for each species using the approach described in Section 2.

Figure 8 shows the ROIs identified by phenology experts, which we used to build and analyze each of the classifiers. In this figure, green areas indicate individuals of the analyzed species, whose SRs obtained from the segmentation were used as positive samples; while red areas represent individuals from the other species, whose the SRs were considered as negative samples.

To assess the effectiveness of each classifier, other individuals (yellow areas; Figure 8) from each of the analyzed species were chosen as a validation set. Then, we used the SRs extracted from those ROIs as input samples for each classifier. Thus, we can measure the classification accuracy as the ratio of the number of samples correctly classified as belonging to the analyzed species to the total number of samples in the validation set.

(a) *Aspidosperma tomentosum*   (b) *Miconia rubiginosa*
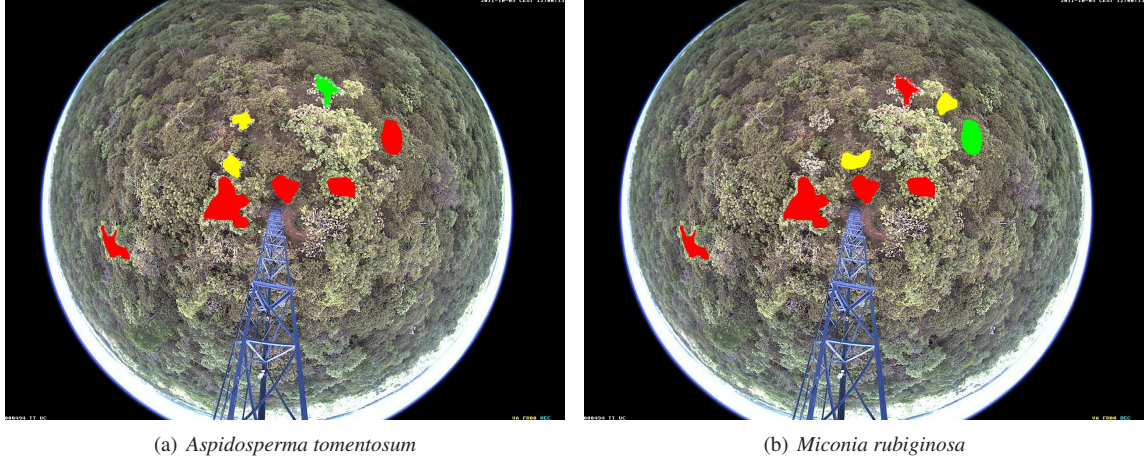
Figure 8: Regions of interest (ROIs) used to build and analyze classifiers: green and red areas indicate individuals of plant species taken, respectively, as positive and negative samples for training; whereas yellow areas indicate individuals of plant species chosen for validation.

4. Results and Discussion

4.1. Classification Accuracy

4.1.1. Color Change Information

Figure 9 shows the classification accuracy for each of the color channels (3 bands: R, G, and B) along all the available periods of the day (13 hours: from 6:00 to 18:00 h), totaling 39 different features for each of the analyzed species.

Figure 10 shows a different view of those results, including all feature combinations, totaling 56 different possibilities. They are: (i) 1 hour of the day and 1 color channel (39 combinations); (ii) 1 hour of the day and all the color channels (13 combinations); (iii) all the hours of the day and 1 color channel (3 combinations); and (iv) all the hours of the day and all the color channels (1 combination). In order to make the comparison easier, we sorted the results from higher to lower accuracy.

Observe that, with less sunshine (early in the morning and late in the afternoon), the classification accuracy is higher, characterizing better the analyzed species for that particular day (Figure 9). It indicates that early and late hours are better to characterize the phenological pattern of plant species for the identification using machine learning. This finding disagrees with the general suggestion of extracting color information from midday hours for ecological studies (Ahrends et al., 2009; Ide and Oguma, 2010; Richardson et al., 2009, 2007). Such differences are related to the type of data analyses being conducted, once those research works are interested in the variation among species (e.g., how different are the phenological patterns of individuals from different species), while the present study is focused on intra-species variations (e.g., how similar are the phenological patterns generated by different individuals of a same species).

Notice also the differences between the behavior of each of the species individually with respect to the color channels, indicating different patterns of leaf color change (Figure 10). This behavior reflects their contrasting leaf phenology (Alberton et al., 2012): the *Miconia rubiginosa* is an evergreen species and, therefore, the leaf senescence is a continuous process and color changes are more subtle over time; in contrast, the *Aspidosperma tomentosum* is deciduous, thus the color change reflects the rapids leaf senescence and the flush of new leaves.

As mentioned in Section 2.2, the MSC approach is based on boosting weak learners. In this paper, each weak learner is a linear SVM classifier using features extracted from a given segmentation scale. In this way, each of the color channels along all the available periods of the day at one of the scales are used as a distinct feature. Table 2 presents the weak classifiers chosen by MSC training algorithm for the *Aspidosperma tomentosum* and *Miconia rubiginosa* species.

Those results confirm that the extreme hours (morning, from 6:00 to 9:00 h; and afternoon, from 15:00 to 18:00 h) are better to characterize plant species. In addition, they also show that the *Aspidosperma tomentosum* and *Miconia rubiginosa* species present a different behavior with respect to the color channels. Moreover, it is interesting to note that coarse scales provide better results than fine ones for the species identification.
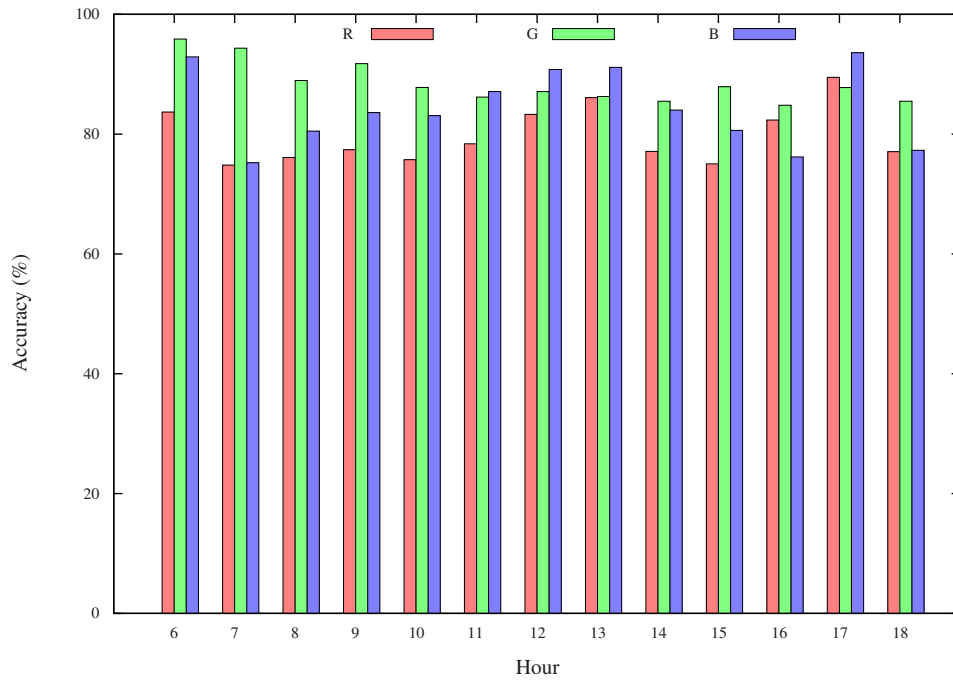
(a) *Aspidosperma tomentosum*
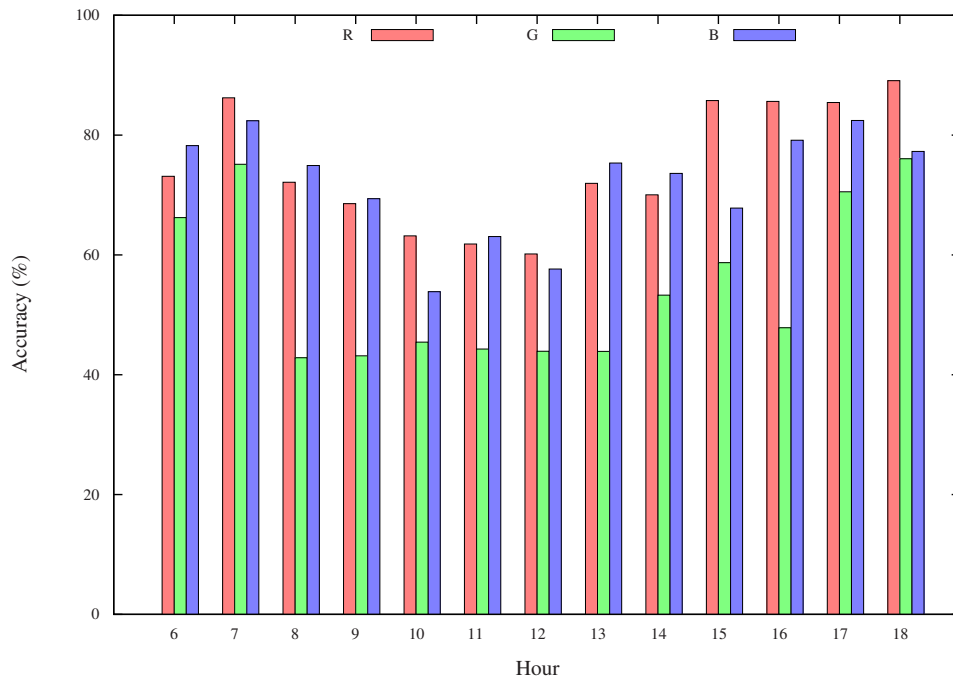
(b) *Miconia rubiginosa*

Figure 9: Classification accuracy for each of the color channels along all the available periods of the day.

(a) *Aspidosperma tomentosum*

(b) *Miconia rubiginosa*

Figure 10: Classification accuracy for each of the color channels along all the available periods of the day (among all the possible combinations).

Table 2: Weak classifiers chosen by the MSC for each round t. The classifier is composed by: color band, hour of the day and segmentation scale.

	Aspidosperma		Miconia rubiginosa	
t	Classifier	Weight	Classifier	Weight
0	7h,R,λ_1	3.9	18h,R,λ_4	4.0
1	16h,B,λ_2	1.0	18h,R,λ_3	3.7
2	16h,B,λ_4	4.1	18h,R,λ_1	1.0
3	16h,R,λ_1	1.0	18h,R,λ_1	1.0
4	7h,B,λ_4	4.6	18h,R,λ_1	1.0
5	7h,B,λ_1	1.0	18h,R,λ_1	1.0
6	7h,B,λ_2	1.0	18h,R,λ_1	1.0
7	16h,B,λ_2	5.2	18h,R,λ_1	1.0
8	7h,B,λ_2	1.0	18h,R,λ_1	1.0
9	7h,B,λ_1	6.3	18h,R,λ_1	1.0

A detailed analysis of the effects of the scale of segmentation on the descriptors is presented in dos Santos et al. (2012a). As pointed out by the authors, all scales are important in different ways: large regions offer more power of description, and the small ones can be used to refine the segmentation.

The reason for the different behavior between the two species is probably related to the leaf change pattern and species functional group. These divergent leafing patterns indicated different behavior for the analyzed species that need further in-depth analyses considering their on-the-ground phenology (Alberton et al., 2012). Based on those results, our analysis suggests that individuals from the same species and functional group can be identified using digital images.

4.1.2. Texture Change Information

Figure 11 shows the classification accuracy for each of the textural metrics (7 statistical measures: mean, variance, contrast, correlation, entropy, homogeneity, and maximum probability) along all the available periods of the day (13 hours: from 6:00 to 18:00 h), totaling 91 different features for each of the analyzed species.

Figure 12 shows a different view of those results, including all the feature combinations, totaling 112 different possibilities. They are: (i) 1 hour of the day and 1 textural metric (91 combinations); (ii) 1 hour of the day and all the textural metrics (13 combinations); (iii) all the hours of the day and 1 textural metric (7 combinations); and (iv) all the hours of the day and all the textural metrics (1 combination). In order to make the comparison easier, we sorted the results from higher to lower accuracy.

In general, the results indicate how promising is the use of textural metrics for capturing phenological patterns, achieving a high classification accuracy, comparable to that from the color features. This opens up a number of possibilities that deserve much deeper study,

but an immediate consequence is that the variation in image texture contains important information which can be explored in phenology studies.

As we can observe, the statistical measures of mean, contrast, and variance achieve the best results for both the *Aspidosperma tomentosum* and *Miconia rubiginosa* species. In contrast, it is interesting to note the differences in responsiveness of each of the species individually with respect to those textural metrics, indicating different patterns of temporal changes in their spatial distribution. The contrast captured better the deciduous leaf change pattern of the *Aspidosperma tomentosum*, as previous described. On the other hand, the mean described better the continuous process of leaf senescence of the *Miconia rubiginosa*, an evergreen species.

The weak classifiers chosen by MSC training algorithm for the *Aspidosperma tomentosum* and *Miconia rubiginosa* species are presented in Table 2. Those results confirm that the statistical measure of mean is better to characterize plant species. In addition, as for the color features, they also show that coarse scales provide better results than fine ones for the species identification.

Table 3: Weak classifiers chosen by the MSC for each round t. The classifier is composed by: textural metric, hour of the day and segmentation scale.
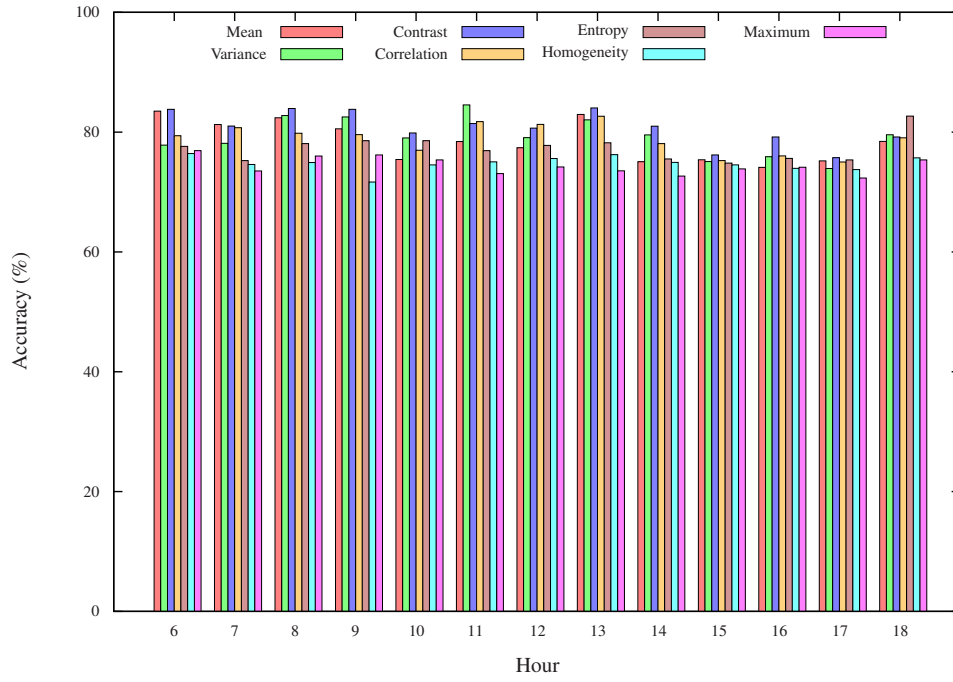
	Aspidosperma		Miconia rubiginosa	
t	Classifier	Weight	Classifier	Weight
0	8h,Variance,λ_1	3.0	7h,Mean,λ_1	1.9
1	7h,Mean,λ_2	3.8	7h,Entropy,λ_2	1.6
2	18h,Mean,λ_1	2.9	17h,Variance,λ_1	1.9
3	7h,Mean,λ_1	4.5	6h,Mean,λ_1	1.7
4	7h,Mean,λ_1	1.0	6h,Mean,λ_1	2.0
5	7h,Mean,λ_1	1.0	6h,Mean,λ_1	2.5
6	7h,Mean,λ_1	1.0	15h,Mean,λ_1	2.9
7	7h,Mean,λ_1	1.0	6h,Mean,λ_1	3.2
8	7h,Mean,λ_1	1.0	6h,Mean,λ_1	1.0
9	7h,Mean,λ_1	1.0	18h,Mean,λ_1	1.0

The strong fine-scale variation in the vegetation leads to a high spectral variation, which is translated into higher variation of textural measures. For that reason, the temporal variation in image texture is an useful information to distinguish plant species.

4.2. Application in Phenology Studies

The species identification in the digital image is a key issue for the near-remote phenological observation of tree crowns, especially in tropical vegetations where one single image may include a high number of species. Usually, this task is very time-consuming since it has to be done in the field, first by matching each crown in the
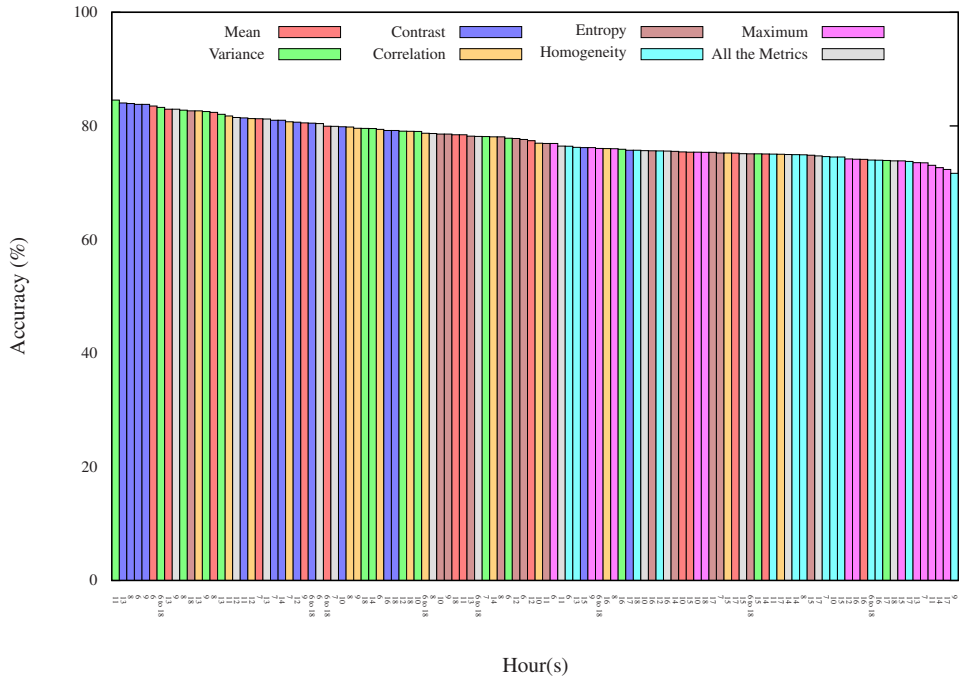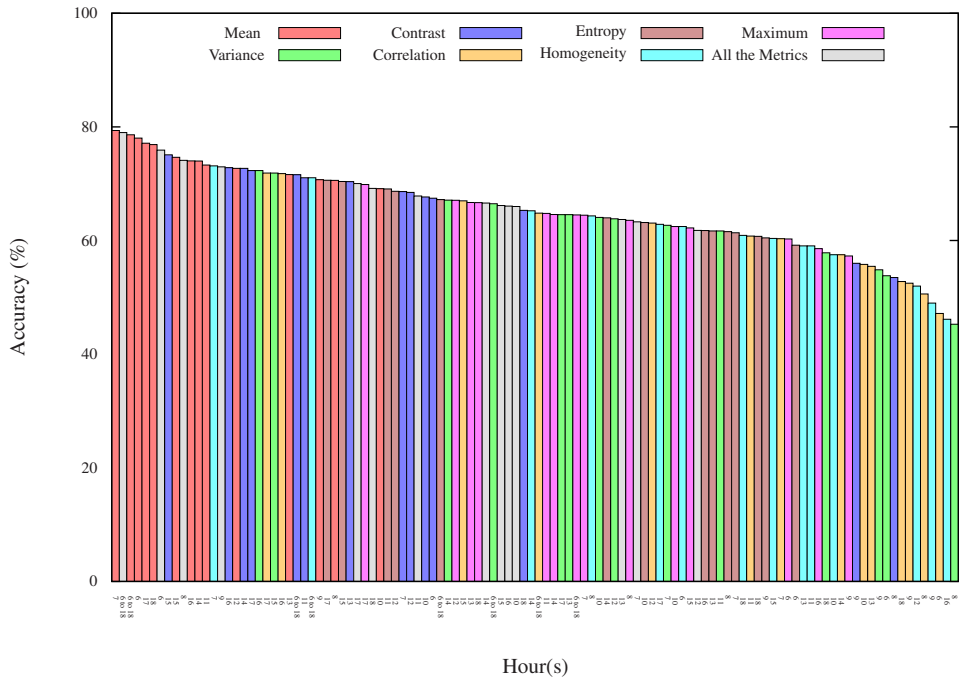
(a) *Aspidosperma tomentosum*
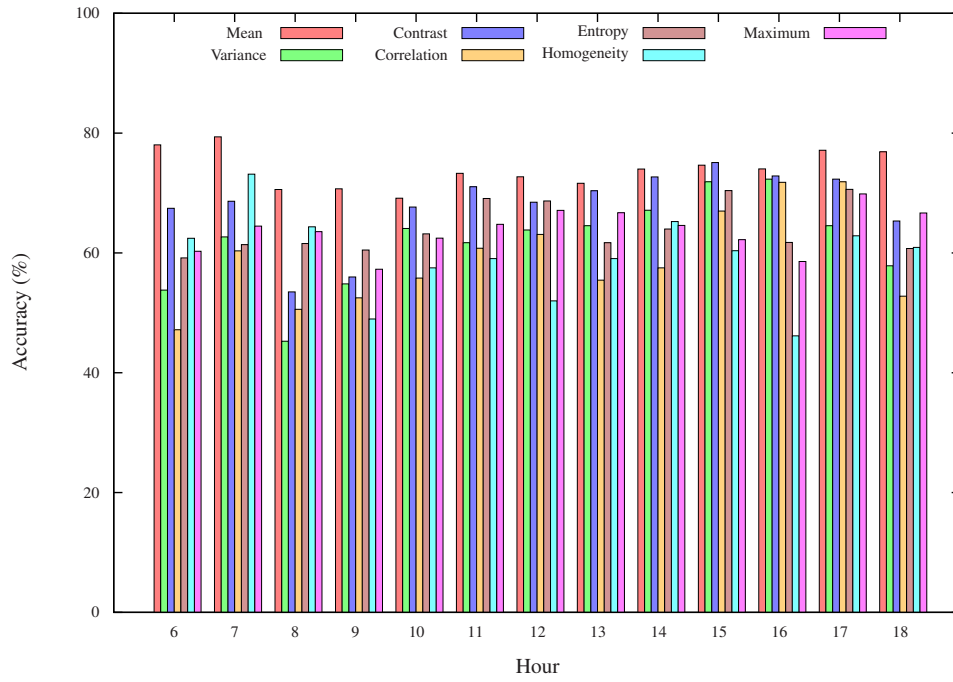
(b) *Miconia rubiginosa*

Figure 11: Classification accuracy for each of the textural metrics along all the available periods of the day.

13

(a) *Aspidosperma tomentosum*

(b) *Miconia rubiginosa*

Figure 12: Classification accuracy for each of the textural metrics along all the available periods of the day (among all the possible combinations).

14

(a) *Aspidosperma tomentosum*
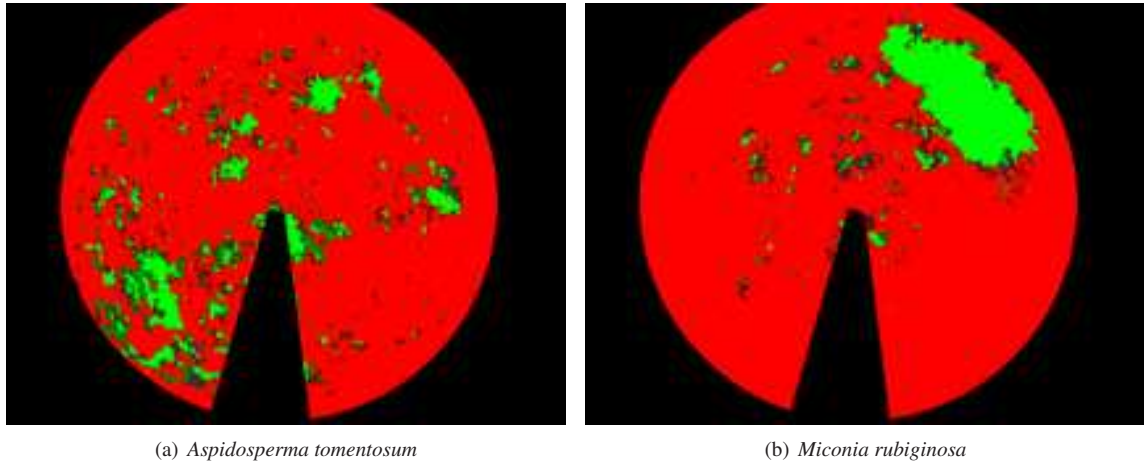
(b) *Miconia rubiginosa*

Figure 13: Image maps produced for different species using the feature combination with the highest classification accuracy. Different color scales were used to maximize the difference between the assigned labels: (i) a green scale, for similar pattens; (ii) a gray scale, for undefined patterns; and (iii) a red scale, for inverted patterns.

image to the tree in the soil and then by identifying the tree at species level.

In this sense, our framework can help phenology experts to find the species in the image, since we can use the MSC approach to automatically identify similar ROIs (tree crowns), reducing the area on the ground over which to look for similar species' ROI, making such a task much easier and faster.

For that, we use the MSC approach to classify segmented regions from the digital images. Next, we create an image map based on the assigned labels, indicating graphically the areas where the probability of finding individuals from a given species is higher.

Figure 13 presents the image maps produced for the analyzed species using the feature combination that achieved the highest classification accuracy (i.e., 6h/G, for the *Aspidosperma tomentosum*; and 6-18h/RGB, for the *Miconia rubiginosa*). Different color scales were used to maximize the difference between the assigned labels: (i) a green scale, for similar pattens (between +1.0 and +0.3); (ii) a gray scale, for undefined patterns (between +0.3 and -0.3); and (iii) a red scale, for inverted patterns[1] (between -0.3 and -1.0).

In this figure, the green areas indicate the segmented regions with a high probability of belonging to the same species. Notice how the search efforts can be greatly reduced by employing our approach. This opens up a number of possibilities that deserve much deeper study, but an immediate consequence is that we can help phe-

nology experts with a new tool to identify plant species, increasing their accuracy on defining the relationship between phenology and climate.

The automatic identification of regions in the digital image with similar phenological patterns have allowed us to find more crowns of the analyzed species, which were validated by the on site identification of the trees. Also, from the point of view of phenology, it has helped us to distinguish different regions in our study area regardless of their individual species and to understand the predominant phenology of a whole community.

5. Conclusions

We conclude that machine learning based on multi-scale classifiers can be applied to detect phenological patterns in the high diversity of the tropical cerrado savanna vegetation. Using a conventional tool to measure the color change information, we were able to define the best hours of the day for characterizing plant species. Different from the suggestion of using midday hours reported in ecological studies, the extreme hours (morning and afternoon) have shown the best results for the species identification using machine learning. Moreover, the data validation at species level have also revealed that different plant species present a different behavior with respect to the color change information. In this way, we were able to distinguish species and functional groups of plants using digital images. Another significant finding of our study was that textural measures exhibit a temporal-change pattern with respect to phenological changes. The potential upside

---

[1]For inverted patterns, we mean a behavior completely opposite of the expected one.

of temporal variation in image texture is that texture differences among multitemporal images contain useful information to characterize plant species. Finally, based on those results, we have introduced a new tool to help phenology experts in the species identification on-the-ground, making such a task much easier and faster. Future work includes the evaluation of other visual features (e.g., color (Almeida et al., 2013) and shape (Torres et al., 2013)) and/or learning methods (e.g., genetic programming (Andrade et al., 2012)).

Acknowledgments

References

Ahrends, H., Etzold, S., Kutsch, W., Stoeckli, R., Bruegger, R., Jeanneret, F., Wanner, H., Buchmann, N., Eugster, W., 2009. Tree phenology and carbon dioxide fluxes: Use of digital photography for process-based interpretation at the ecosystem scale. Climate Research 39, 261–274.

Alberton, B., Almeida, J., Henneken, R., Torres, R. S., Menzel, A., Morellato, L. P. C., 2012. Near remote phenology: Applying digital images to monitor leaf phenology in a brazilian cerrado savanna. In: International Conference on Phenology (Phenology'12). p. 2.

Almeida, J., dos Santos, J. A., Alberton, B., Morellato, L. P. C., Torres, R. S., 2013. Visual rhythm-based time series analysis for phenology studies. In: IEEE International Conference on Image Processing (ICIP'13). pp. 1–5.

Almeida, J., dos Santos, J. A., Alberton, B., Torres, R. S., Morellato, L. P. C., 2012. Remote phenology: Applying machine learning to detect phenological patterns in a cerrado savanna. In: IEEE International Conference on eScience (eScience'12). pp. 1–8.

Alpaydin, E., 2010. Introduction to Machine Learning. Adaptive Computation and Machine Learning. MIT Press.

Andrade, F. S. P., Almeida, J., Pedrini, H., da S. Torres, R., 2012. Fusion of local and global descriptors for content-based image and video retrieval. In: Iberoamerican Congress on Pattern Recognition (CIARP'12). pp. 845–853.

Cheng, H.-D., Jiang, X., Sun, Y., Wang, J., 2001. Color image segmentation: Advances and prospects. Pattern Recognition 34 (12), 2259–2281.

Cope, J. S., Corney, D. P. A., Clark, J. Y., Remagnino, P., Wilkin, P., 2012. Plant species identification using digital morphometrics: A review. Expert Systems with Applications 39 (8), 7562–7573.

Coutinho, L. M., 1978. O conceito de cerrado. Brazilian Journal of Botany 1, 17–23.

Culbert, P. D., Pidgeon, A. M., St.-Louis, V., Bash, D., Radeloff, V. C., 2009. The impact of phenological variation on texture measures of remotely sensed imagery. IEEE Journal of Selected Topics in Applied Earth Observations and Remote Sensing 2 (4), 299–309.

dos Santos, J. A., Faria, F. A., Torres, R. S., Rocha, A., Gosselin, P.-H., Philipp-Foliguet, S., Falcão, A. X., 2012a. Descriptor correlation analysis for remote sensing image multi-scale classification. In: IEEE International Conference on Pattern Recognition (ICPR'01). pp. 1–4.

dos Santos, J. A., Gosselin, P.-H., Philipp-Foliguet, S., da S. Torres, R., Falcão, A. X., 2012b. Multi-scale classification of remote sensing images. IEEE Transactions on Geoscience and Remote Sensing 50 (10), 3764–3775.

Grabner, H., Bischof, H., 2006. On-line boosting and vision. In: IEEE International Conference on Computer Vision and Pattern Recognition (CVPR'06). pp. 260–267.

Guigues, L., Cocquerez, J., Le Men, H., 2006. Scale-sets image analysis. International Journal of Computer Vision 68, 289–317.

Haralick, R. M., Shanmugam, K., Dinstein, I., 1973. Textural features for image classification. IEEE Transaction on Systems, Man and Cybernetics 3 (6), 610–621.

Ide, R., Oguma, H., 2010. Use of digital cameras for phenological observations. Ecological Informatics 5, 339–347.

Keeling, C. D., Chin, J. F. S., Whorf, T. P., 1996. Increased activity of northern vegetation inferred from atmospheric co2 measurements. Nature 382, 146–149.

Kumar, N., Belhumeur, P. N., Biswas, A., Jacobs, D. W., Kress, W. J., Lopez, I. C., Soares, J. V. B., 2012. Leafsnap: A computer vision system for automatic plant species identification. In: European Conference on Computer Vision (ECCV'12). pp. 502–516.

Kurc, S., Benton, L., 2010. Digital image-derived greenness links deep soil moisture to carbon uptake in a creosotebush-dominated shrubland. Journal of Arid Environments 74, 585–594.

Lechervy, A., Gosselin, P.-H., Precioso, F., 2013. Boosted kernel for image categorization. Multimedia Tools and Applications.

Loustau, D., Bosc, A., Colin, A., Davi, H., François, C., Dufrêne, E., Équé, M., Cloppet, E., Arrouays, D., Le Bas, C., Saby, N., Pignard, G., Hamza, N., Granier, A., Breda, N., Ciais, P., Viovy, N., Ogée, J., Delage, J., 2005. Modeling the climate change effects on the potential reduction of french plains forests at the sub regional level. Tree Physiol 25, 813–823.

Morellato, L. P. C., Rodrigues, R. R., Leitão Filho, H. F., Joly, C. A., 1989. Estudo comparativo da fenologia de espécies arbóreas de floresta de altitude e floresta mesófila semidecídua na serra do iapí, jundiaí, são paulo. Brazilian Journal of Botany 12, 85–98.

Nagai, S., Maeda, T., Gamo, M., Muraoka, H., Suzuki, R., Nasahara, K. N., 2011. Using digital camera images to detect canopy condition of deciduous broad-leaved trees. Plant Ecology and Diversity 4, 79–89.

Negi, G. C. S., 2006. Leaf and bud demography and shoot growth in evergreen and deciduous trees of central himalaya, india. Trees 20, 416–429.

Parmesan, C., Yohe, G. A., 2003. A globally coherent fingerprint to climate change impacts accross natural systems. Nature 421, 37–42.

Reich, P. B., 1995. Phenology of tropical forests: Patterns, causes and consequences. Canadian Journal of Botany 73, 164–174.

Reys, P., 2008. Estrutura e fenologia da vegetação de borda e interior em um fragmento de cerrado *Sensu Stricto* no sudeste do brasil (itirapina, são paulo). Ph.D. thesis, Bioscience Institute, Sao Paulo State University, Rio Claro, SP, Brazil.

Richardson, A. D., Braswell, B. H., Hollinger, D. Y., Jenkins, J. P., Ollinger, S. V., 2009. Near-surface remote sensing of spatial and temporal variation in canopy phenology. Ecological Applications 19, 1417–1428.

Richardson, A. D., Jenkins, J. P., Braswell, B. H., Hollinger, D. Y., Ollinger, S. V., Smith, M. L., 2007. Use of digital webcam images to track spring greep-up in a deciduous broadleaf forest. Oecologia 152, 323–334.

Rosenzweig, C., Karoly, D., Vicarelli, M., Neofotis, P., Wu, Q., Casassa, G., Menzel, A., Root, T. L., Estrella, N., Seguin, B., Tryjanowski, P., Liu, C., Rawlins, S., Imeson, A., 2008. Attributing physical and biological impacts to anthropogenic climate change. Nature 453, 353–357.

Rostamizadeh, A., Talwalker, A., 2012. Foundations of Machine Learning. Adaptive Computation and Machine Learning Series. University Press Group Limited.

Rotzer, T., Grote, R., Pretzsch, H., 2004. The timing of bud burst and its effect on tree growth. International Journal of Biometeorology 48, 109–118.

Schapire, R. E., 1999. A brief introduction to boosting. In: Dean, T. (Ed.), International Joint Conference on Artificial Intelligence (IJCAI'99). pp. 1401–1406.

Schwartz, M. D., 2003. Phenology: An Integrative Environmental Science. Academic Publishers.

Schwartz, M. D., Reed, B. C., White, M. A., 2002. Assessing satellite derived start-of-season measures in the coterminous. International Journal of Climatology 22, 1793–1805.

Staggemeier, V. G., Diniz-Filho, J. F., Morellato, L. P. C., 2010. The shared influence of phylogeny and ecology on the reproductive patterns of Myrteae (Myrtaceae). Journal of Ecology 98, 1409–1421.

Tan, P.-N., Steinbach, M., Kumar, V., 2005. Introduction to Data Mining. Addison-Wesley.

Torres, R. S., Falcão, A. X., 2006. Content-based image retrieval: Theory and applications. Revista de Informática Teórica e Aplicada 13 (2), 161–185.

Torres, R. S., Hasegawa, M., Tabbone, S., Almeida, J., dos Santos, J. A., Alberton, B., Morellato, L. P. C., 2013. Shape-based time series analysis for remote phenology studies. In: IEEE International Geoscience and Remote Sensing Symposium (IGARSS'13). pp. 1–4.

Unser, M., 1986. Sum and difference histograms for texture classification. IEEE Transactions on Pattern Analysis and Machine Intelligence 8 (1), 118–125.

Viola, P., Jones, M., 2001. Rapid object detection using a boosted cascade of simple features. In: IEEE International Conference on Computer Vision and Pattern Recognition (CVPR'01). pp. 511–518.

Walther, G. R., 2004. Plants in a warmer world. Perspectives in Plant Ecology Evolution and Systematics 6, 169–185.

Walther, G. R., Post, E., Convey, P., Menzel, A., Parmesan, C., Beebee, T. J. C., Fromentin, J. M., Hoegh-Guldberg, O., Bairlein, F., 2002. Ecological responses to recent climate change. Nature 416, 389–395.

White, M. A., Running, S. W., Thornton, P. E., 1999. The impact of growing-season length variability on carbon assimilation and evapotranspiration over 88 years in the eastern us deciduous forest. International Journal of Biometeorology 42, 139–145.